Fundamental Studies on Electron Beam Welding of Heat-resistant Superalloys for Nuclear Plants (Report I)†

— Effect of Welding Conditions on Some Characteristics of Weld Bead —

Yoshiaki ARATA*, Kiyohide TERAI**, Hiroyoshi NAGAI**, Shigeki SHIMIZU** and Toshiichi AOTA**

Abstract

In this paper, the effect of the welding conditions on the characteristics of the weld geometry and the weld defects was made clear, concerning the heat-resistant superalloys for the nuclear plants. Obtained conclusion may be summarized as follows, using technical symbols which are given meanings in this report.

1) The weld defects were R-porosity and microcrack.

2) S_p and Δa_b are considered to be the important criteria for the evaluation of the susceptibility to the R-porosity.

3) Superalloys could be evaluated in the sensitivity to the microcrack in terms of the critical heat input to avoid microcrack q_{cr}. This q_{cr} is considered to be one of the proper criteria for evaluating the superalloys in the susceptibility to the microcrack.

4) Most microcracks were apt to occur when h_c/h_N came near to 1.0. These microcracks came to occur easily with the increase of $d_{B\cdot N}/d_B$.

1. Introduction

In recent years, such superalloys as Hastelloy type, Inconel type, Incoloy type, etc. have been taken into consideration as one of the materials for very high temperature gas-cooled reactor, where dimensional tolerance is strictly limited from the structural viewpoint for the safety assurance peculiar to the nuclear plants and the strength at very high temperatures is also required. In this sense, welding of these superalloys involves many problematical points.

As it is well recognized that the energy density in the electron beam welding process is extremely high by nature, the large penetration depth can be easily obtained with small heat input. Furthermore, very precise welding can be performed at high quality in the vacuum chamber. For these reasons, electron beam welding seems to be most suitable for welding of the heat-resistant superalloys for the nuclear plants. However, very rapid melting of the limited area with the heat source of high energy density tends to cause such individual weld defects as porosity, cold shut, spiking and cracking. There are some fundamental reports[1)~5)] on these weld defects. However, there is no report on these weld defects of the superalloys.

As described above, weld defects in the electron beam welds of these superalloys have not been clarified yet. In this report, authors herein determined the effect of the welding conditions on some characteristics of weld bead, that is, the weld geometry and the weld defects by the slope welding method to establish the proper welding conditions for these superalloys.

2. Material and Experimental Instrument used

Such superalloys as Hastelloy type, Inconel type and Incoloy type and austenitic stainless steel for compararison were used which generally seem to be fit for very high temperature gas-cooled reactor. Chemical composition and mechanical properties of these superalloys are shown in Table 1. Brief marks shown in Table 1 are below employed to distinguish Hastelloy X of different heat. Welding of these materials was conducted by 150kV-40mA type electron beam welder of hard vacuum.

3. Experimental Procedure

20mm-thick materials shown in Table 1 were set on work table as in Fig. 1, where slope angle θs equals 30°. Thereafter, upslope welding was performed with the electron gun fixed, moving work table in such a direction as arrow shows. In this case, a_b parameter[6)] defined by D_O/D_F (where, D_O: object distance, D_F: focal length)

† Received on Sep. 24, 1976

* Professor

** Kawasaki Heavy Industries, Ltd., Japan

Table 1 Chemical Composition and Mechanical Properties of Superalloys used

Material	Mark	Thickness (mm)	Melting Process*	Final Heat Teatment	Grain Size (ASTM)	Mechanical Properties				Chemical Composition (%)																Gaseous Contents (ppm)			
						0.2%PS	TS	El. (%)	R of A (%)	C	Si	Mn	P	S	Ni	Cr	Co	Mo	W	Nb (+Ta)	Al	Ti	B	Zr	Ce	Fe	O	N		
																												Sol.	Insol	Total
Hastelloy X	HAEN	20	AE	1120°C×18Min WQ	1~4	30.4	71.1	59.0	65.0	0.6	0.48	0.88	0.016	<0.02	Bal.	21.4	1.77	9.05	0.45		0.07	0.15	0.002			19.1	3	405	42	447
	HAEM			1150°C×50Min WQ	5~6	38.7	75.0	47.0	—	0.08	0.37	0.59	0.012	<0.02		20.7	10.3	8.70	0.50	—	0.21	0.02	0.001	—	—	18.2	2	248	20	268
	HVEN		VE	1120°C×18Min WQ	1~4	34.3	73.8	49.3	56.9	0.04	0.17	0.04	0.010	<0.02		20.7	15.9	9.20	0.55		0.002	0.19	0.002			18.5	5	306	16	322
	HVERN			1170°C×30Min AC	1~4	32.4	74.0	54.3	52.2	0.05	0.35	0.72	0.010	<0.02		21.4	14.5	8.93	0.51	0.05	0.005	0.006	2.0	9	≤5	19.1	4	121	22	143
Inconel 625	Inl 625AE		AE	1000°C×1Hr WQ	6	45.5	90.1	46.8	—	0.03	0.28	0.24	0.010	<0.02		22.1	0.06	8.81	0.69	3.53	0.24	0.13	—	—	—	2.54	3	44	211	255
Inconel 617	Inl 617 V		V	1170°C×1Hr WQ	3~4	30.0	74.6	70.0	57.0	0.06	0.17	0.02	0.010	<0.02		21.2	12.6	9.00	—	—	0.93	0.52	—	—	—	1.45	4	244	180	424
Incoloy 800	Iny 800V		V	1100°C×15Hr WQ	2.5	22.1	58.2	52.0	72.1	0.06	0.37	0.77	0.010	0.002	32.1	21.2	0.50	0.01	0.8	—	—	0.51	0.59	—	—	—		6	32	93	125
Incoloy 807	Iny 807A		A	1230°C×3Hr WQ	1~3	25.7	64.1	52.2	60.3	0.07	0.50	0.70	0.020	0.002	40.1	20.6	8.28	0.20	4.85	0.99	0.47	0.024	—	—	—	Bal.	—	68	144	212
SUS 316	S 316		A	1100°C×13Min WQ	3~5	—	60.3	61.4	—	0.05	0.79	1.26	0.028	0.004	11.5	17.5	—	2.58	—	—	—	—	—	—	—		13	257	32	289

*AE: Air Melting followed by Electroslag Remelting, VE: Vacuum Induction Melting followed by Electroslag Remelting
V: Vacuum Induction Melting, A: Air Melting

is called "beam active parameter" or "active parameter" which is one of the important variables in the electron beam welding. As max. penetration depth is experimentally clarified to be obtained around the a_b parameter of 0.9, materials were set so that the a_b parameter might agree precisely with this value at the center line C-C in Fig. 1. This enables a_b parameter to vary over considerably wide range from 0.6 to 1.2.

After the bead-on-plate welding, X-ray inspection was carried out by such a method as shown in Fig. 2 to investigate the weld defects. Thereafter, every bead-on-plate weld was machined so that transverse profile might be microscopically inspected after polishing and etching. Thereby, penetration depth and bead width were respectively measured. Microcrack was also investigated by the microscope.

The diameter of the electron beam was measured by means of the AB-test (Arata Beam Test)[7].

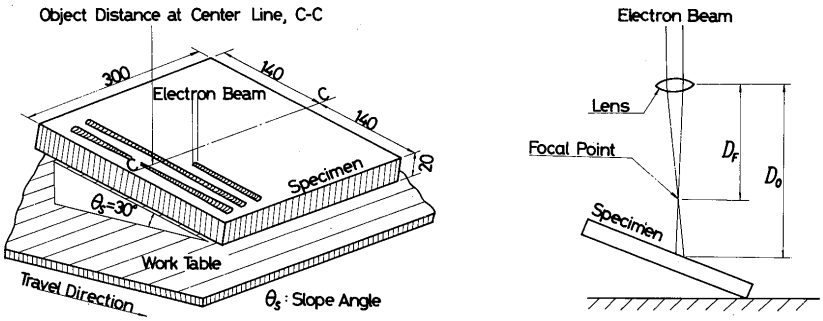

Fig.1 Bead-on-plate Welding Method by Slope Welding

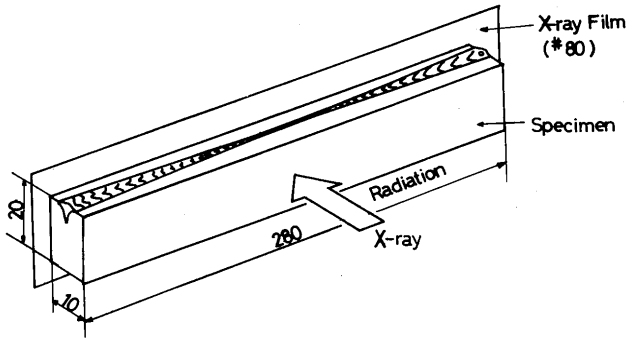

Notes
1. Specimen is machined from bead-on-plate welds.
2. *80 means film sensitivity.
3. X-ray film is apart from X-ray Source by 600mm approximately.

Fig.2 X-ray Inspection Method of Bead-on-plate Welds

4. Experimental Result and Discussion

It was recognized through the X-ray inspection and microscopical survey that porosity and microcrack were observed in almost all the materials. These results are described in details below.

4.1 Porosity

Porosity observed in X-ray inspection was root porosity (R-porosity) to occur at the root of the penetration. Typical R-porosity is shown in Photo. 1.

It is reported that occurrence of the R-porosity depends upon the heat input[1]. In this experiment, occurrence of the R-porosity is arranged on $w_B (= \frac{I_b V_b}{2 r_b v_b})$ – a_b diagram (where, I_b: beam current, V_b: accelerating voltage, r_b: radius of the electron beam, v_b. welding speed). Above-mentioned w_B is herein defined as the "bead energy density" of the electron beam, that is, the heat input divided by the actual beam diameter of the electron beam, which means the energy density of the electron beam supplied on the surface of the material.

V_b=150kV
I_b =40mA
v_b'=160cm/min
a_b =0.87

Photo. 1 Typical R-porosity (SUS 316)

As far as it concerns with the electron beam welding, the diameter of the electron beam is very dependent both upon the welding conditions and upon the type itself of the electron beam welder. Therefore, estimation of the proper welding conditions and comparison of the susceptibility to the porosity are considered to be done in any case by use of the diagram proposed above.

Figs. 3 and 4 show the examples of w_B–a_b diagram concerning the occurrence of the R-porosity. It was noted on the curve of the constant heat input whether R-porosity did occur or not. As a result, R-porosity was recognized to occur within the certain range of a_b parameter. When the penetration depth and heat input are limited less than 15mm and 5000 joule/cm (I_b : 40mA, V_b : 125kV, v_b': 60 cm/min) respectively, the area where R-porosity occurs can be shown as in the figures by plotting these critical a_b parameter on the curve of the constant heat input. In these figures, the penetration depth is constant on the certain curve. In other expression, h_p=15mm means that penetration depth is constantly 15mm on this curve.

Susceptibility to the R-porosity might be evaluated by above-mentioned individual area S_p, max. bead energy density $w_{B.m}$ and the difference of the critical a_b parameters, that is, $\Delta a_b (\equiv a_{b.2} - a_{b.1})$ as shown in Fig. 5. Herein, smaller S_p and Δa_b and larger $w_{B.m}$ means less susceptibility to the R-porosity.

Table 2 evaluates the susceptibility of the superalloys to the R-porosity in terms of these criteria, S_p, $w_{B.m}$ and Δa_b. As shown in this table, there is appreciable difference among the superalloys in terms of S_p and Δa_b. There is also clear correlation between S_p and Δa_b. It may be safely said from these results that the susceptibility of the superalloys to the R-porosity is evaluated in terms of S_p and Δa_b. Generally speaking, Fe-base superalloys such as Incoloy 800 and austenitic stainless steel (SUS316) are more susceptible to the R-porosity as compared with Ni-base superalloys such as Hastelloy X, Inconel 625.

Table 2 Criteria obtained for Evaluation of Susceptibility to R-porosity

Material	$S_p/S_{p.m}$	$w_{B.m}$ (joule/cm²)	$a_{b.1}$	$a_{b.2}$	Δa_b
Hastelloy X (HAEN)	0.75	2.35	0.83	1.08	0.25
Hastelloy X (HAEM)	0.66	2.35	0.89	1.09	0.20
Hastelloy X (HVEN)	0.60	2.35	0.87	1.07	0.20
Hastelloy X (HVERN)	0.73	2.95	0.85	1.09	0.24
Inconel 625 (Inl 625AE)	0.75	2.35	0.78	1.13	0.35
Inconel 617 (Inl 617V)	1.00	1.26	0.71	1.16	0.45
Incoloy 800 (Iny 800V)	0.91	2.95	0.69	1.12	0.43
Incoloy 807 (Iny 807)	0.55	2.95	0.81	1.09	0.28
SUS 316 (S 316)	0.91	1.89	0.71	1.16	0.45

S_p means the area schematically shown in Fig. 5 where R-porosity occurs.
$S_{p.m}$ means max. S_p in this experiment.

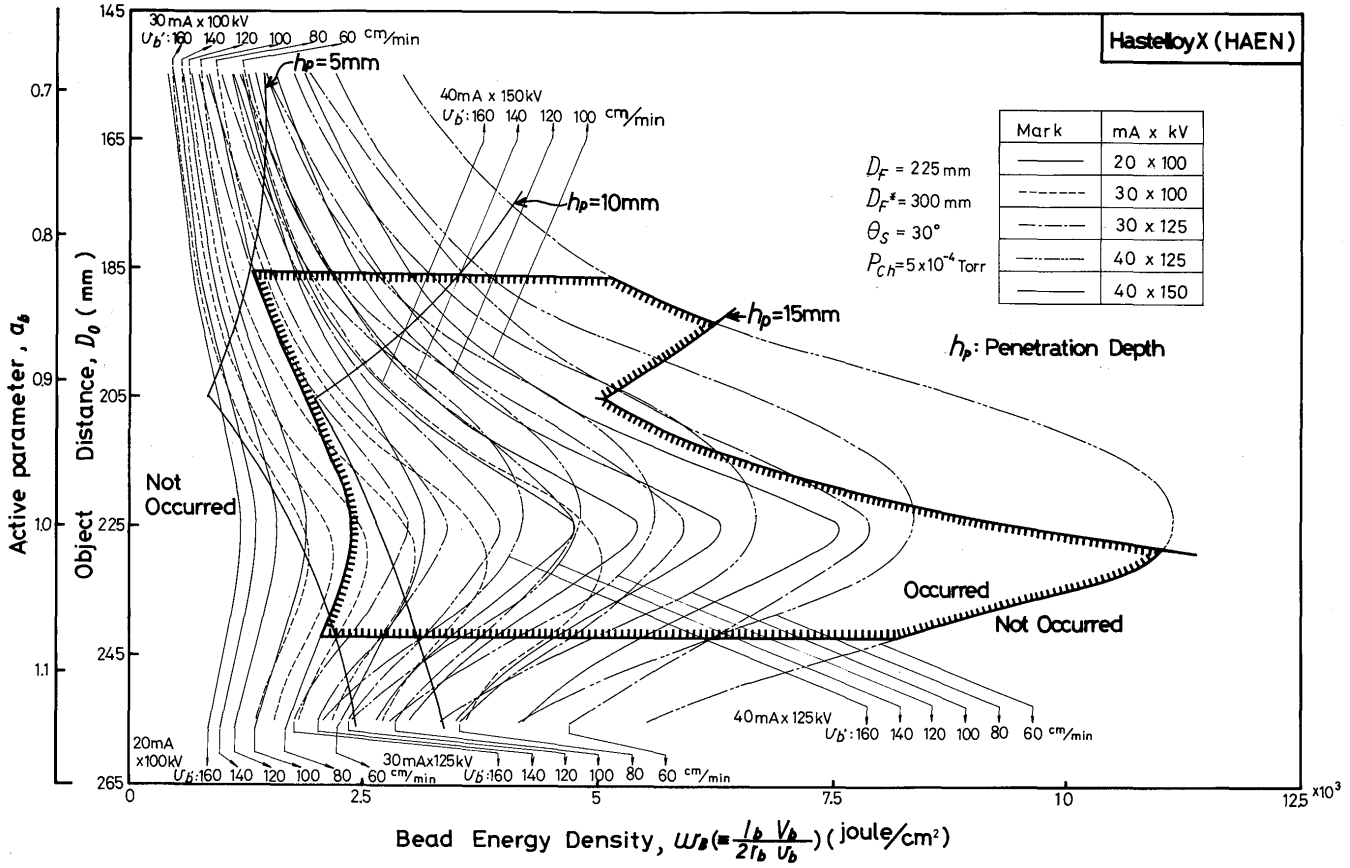

Fig.3 Effect of Bead Energy Density and Active Parameter on R-porosity

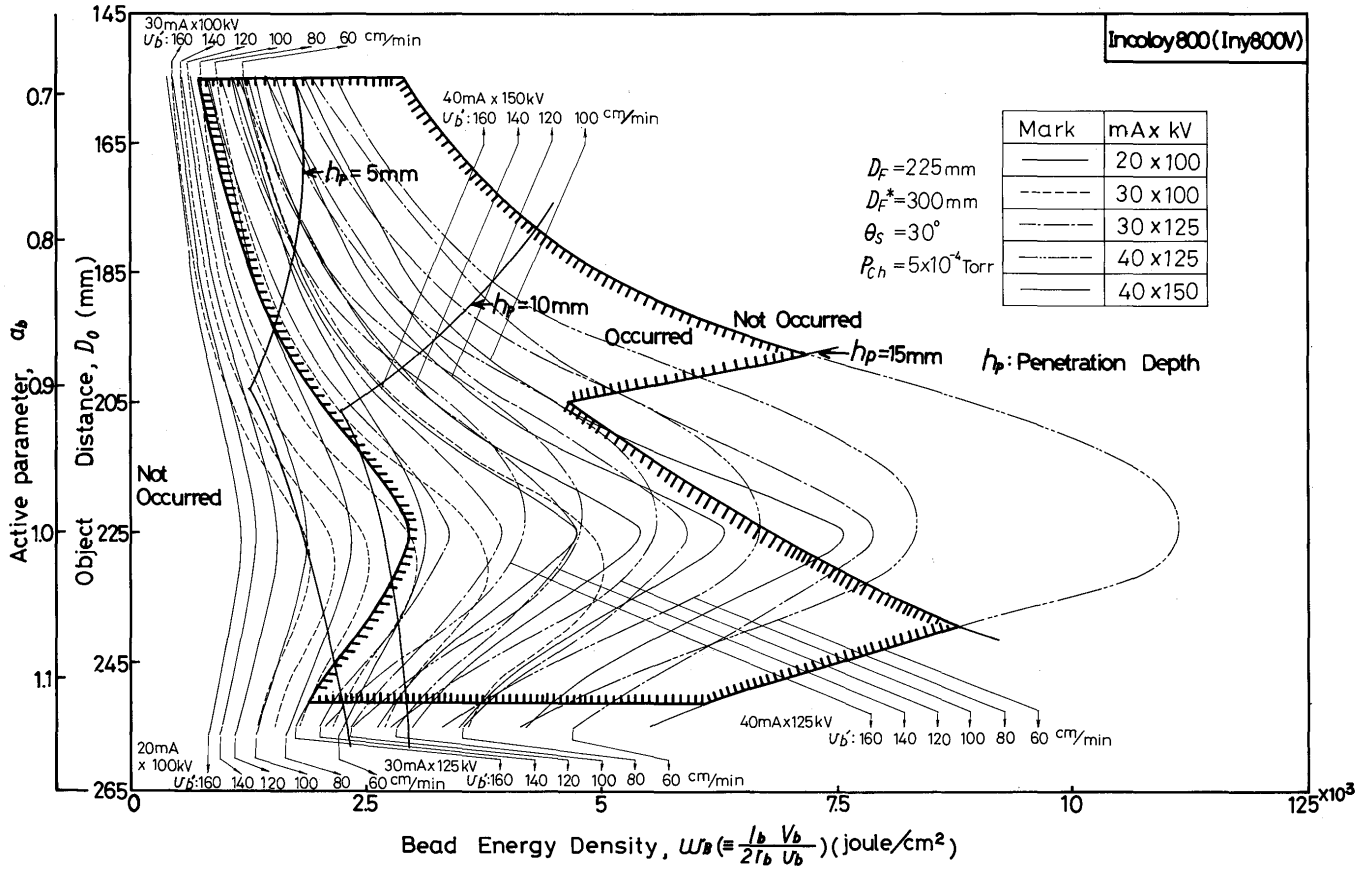

Fig. 4 Effect of Bead Energy Density and Active Parameter on R-porosity

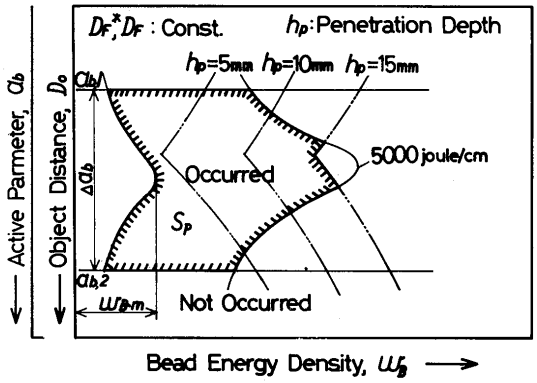

Fig. 5 Evaluating Criteria for R-porosity

4.2 Microcracking

Every transverse cross section was electrolitically polished with the mixed solution (1.5% perchloric acid, 5.7% sodium thiocyanate, 7.1% citric acid, 75.5% ethyl alcohol, 9.4% N-propyl alcohol and 0.8% oxine in weight percent) and also etched with 10% oxalic acid solution. Thereafter, microcrack in the electron beam welds was investigated through the microscopic survey.

Microcrack was observed in the electron beam welds of all the superalloys except for Inconel 625 and SUS316. In most cases, microcrack was continuously seen in the interdendritic boundary of weld metal and the grain boundary of heat affected zone and also nearly perpendicular to the fusion boundary. Typical microcrack is shown in Photo. 2.

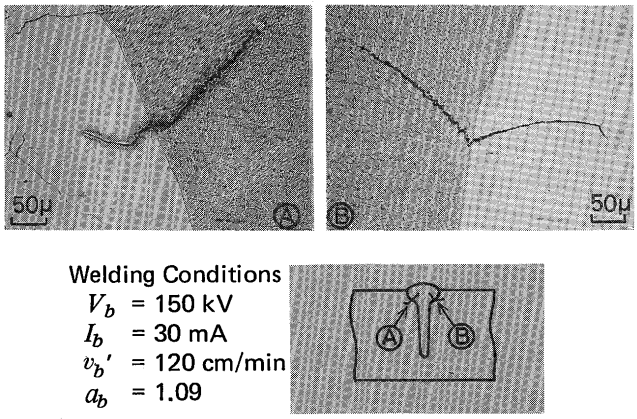

Photo. 2 Typical Microcrack (Hastelloy X, HAEN)

(1) Effect of Power of Electron Beam and Welding Speed on Microcrack

Fig. 6 shows the effect of the power of electron beam $W_b(\equiv I_b V_b)$ and the welding speed v_b' on the occurrence of the microcrack in the superalloys. On this $w_b - v_b'$ diagram, there is drawn the critical line on the disappearance of the microcrack. It can be said from this figure that microcrack is completely prevented in this experiment by limiting the welding conditions in consideration of this critical line. Furthermore, these critical lines are nearly parallel to one another. From this result, it can be considered that the superalloys are not so susceptible to the microcrack in which microcrack never occur in a larger region. The superalloys are below placed in terms of this region in the order of less susceptibility to the microcrack.

(SUS316, Inconel 625), HAEM, HAEN, Incoloy 800, HVEN, (HVERN, Inconel 617)

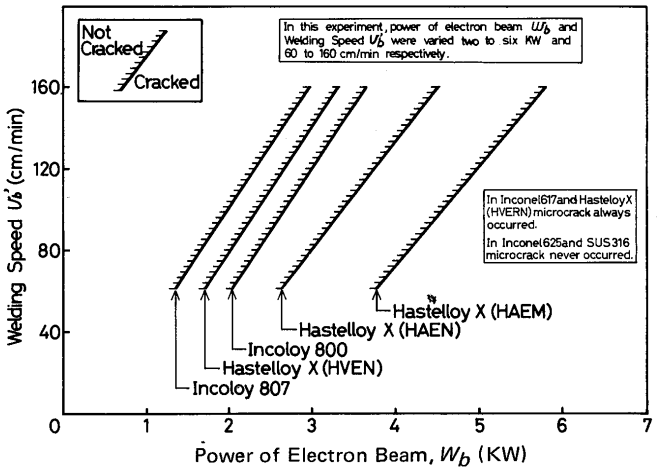

Fig. 6 Effect of Power of Electron Beam and Welding Speed on Microcrack

(2) Effect of Heat Input on Microcrack

Fig. 7 shows the example of the relation between the heat input and microcracking percentage (cracked specimens' ratio of all the specimens at the constant heat input). From this figure, microcracking percentage tends to increase with the increase of the heat input and the microcrak disappear at the heat input less than the certain value. This value of every superalloy, under which microcrack never occurs, can be regarded as the critical heat input to avoid microcrack q_{cr} which is tabulated in Table 3. That is to say, q_{cr} is one of the important criteria to evaluate the superalloys in the susceptibility to the microcrack. In this table, max. heat input in this experiment are used as the critical heat input to avoid microcrack for Inconel 625 and SUS316 in which microcrack never occurred. On the other hand, minimum one is also used as that for Inconel 617 and HVERN in which microcrack invariably occurred. In terms of q_{cr}, the superalloys are below placed in the order of less susceptibility to the microcrack.

(SUS316, Inconel 625), HAEM, HAEN. (HVEN, Incoloy 800) Incoloy 807, (HVERN, Inconel 617)

This order agrees nearly with the above-mentioned one.

Microcrack was widely scattered with considerable irregularity on the $w_B - a_b$ diagram. Therefore, it was

difficult to clarify the effect of W_B and a_b parameter on the microcrack. Generally speaking, however, microcrack was apt to disappear both around a_b parameter of 0.9 and with the decrease of bead energy density W_B.

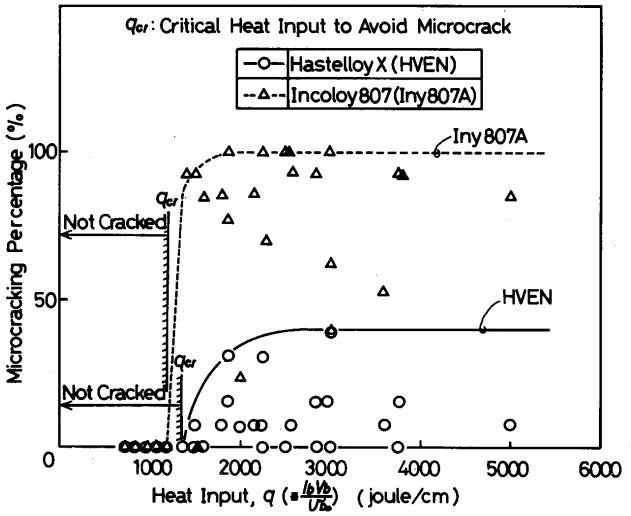

Fig. 7 Effect of Heat Input on Microcracking

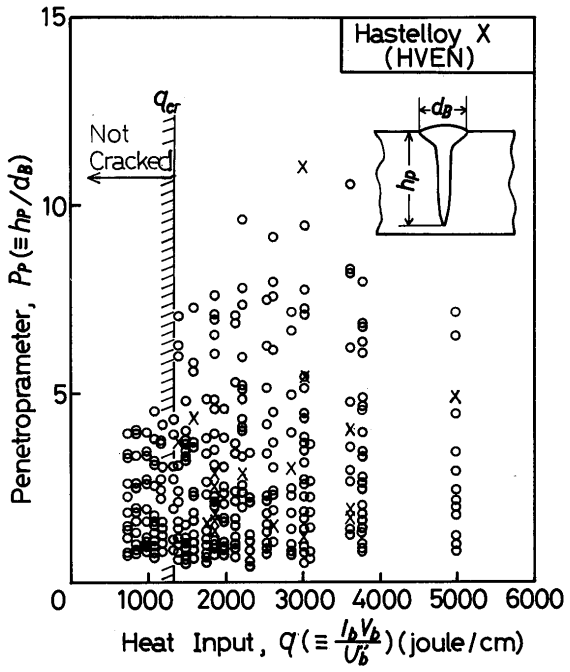

Fig. 8 Effect of Heat Input and Penetroparameter on Microcrack

Table 3 Critical Heat Input to Avoid Microcrack

Material	q_{cr} (joule/cm)
Hastelloy X (HAEN)	1406
Hastelloy X (HAEM)	2143
Hastelloy X (HVEN)	1286
Hastelloy X (HVERN)	< 750
Inconel 625 (Inl 625AE)	> 5080
Inconel 617 (Inl 617V)	< 750
Incoloy 800 (Iny 800V)	1286
Incoloy 807 (Iny 807A)	1200
SUS 316 (S 316)	> 5080

q_{cr}: Critical Heat Input to Avoid Microcrack

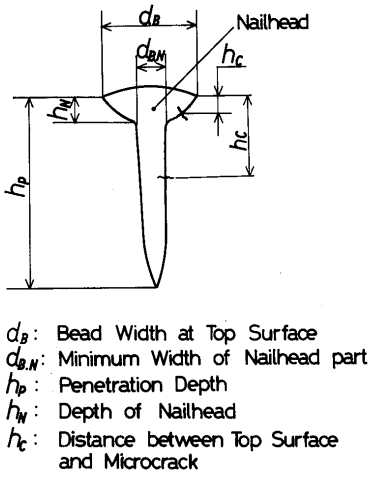

Fig. 9 Electron Beam Weld Geometry defined

(3) Correlation between Microcrack and Penetroparameter

Fig. 8 shows the example of the effect of heat input and penetroparameter P_P ($\equiv h_p/d_B$, h_P: penetration depth, d_B: bead width) on the microcrack. In every cracked superalloy, there was no definite effect of P_P value on the microcrack. As described above, there was clear correlation between the microcrack and the heat input. In this figure, there is also recognized the critical heat input to avoid microcrack. This corresponds to q_{cr} described above.

(4) Position of Microcrack

Typical geometry of the electron beam welds is herein defined as shown in Fig. 9 to make the microcrack clearer in its position. Every microcrack was carefully examined in its position by the microscope.

Figs. 10 to 12 show typical examples in which the microcrack is plotted on h_N/h_P–h_c/h_N diagram (where, h_N: depth of the nailhead, h_P: penetration depth, h_c: distance between the top surface and the position of microcrack). Inconel 617, HVERN and Incoloy 807, very sensitive to the microcrack, had quite similar features in its position. In case of Inconel 617, most microcracks are

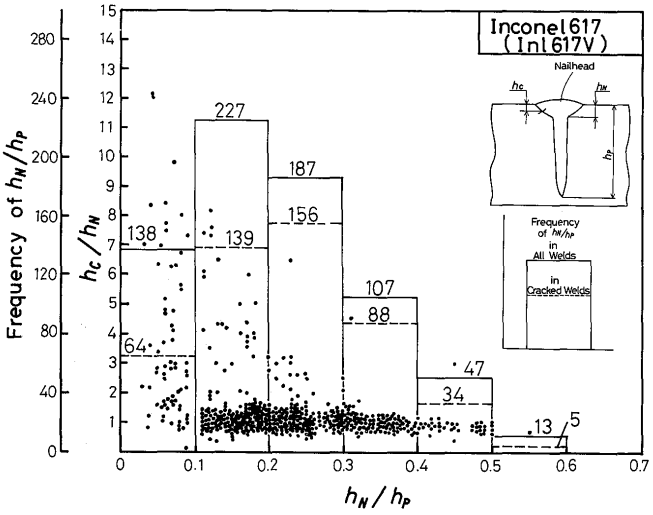

Fig. 10 Effect of h_N/h_P and h_c/h_N on Microcrack

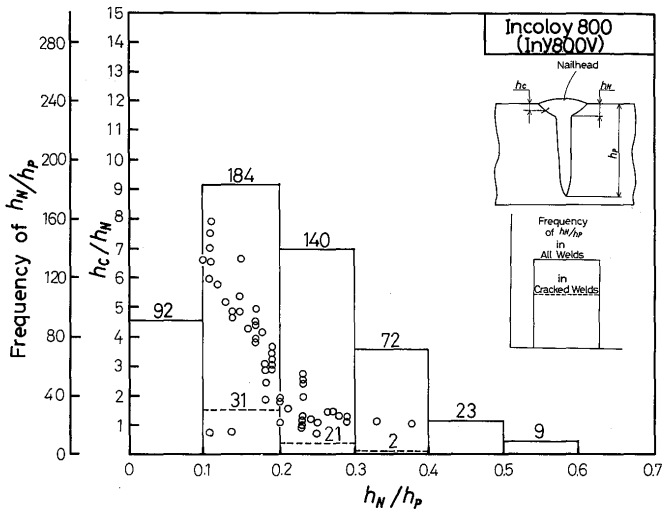

Fig. 12 Effect of h_N/h_P and h_c/h_N on Microcrack

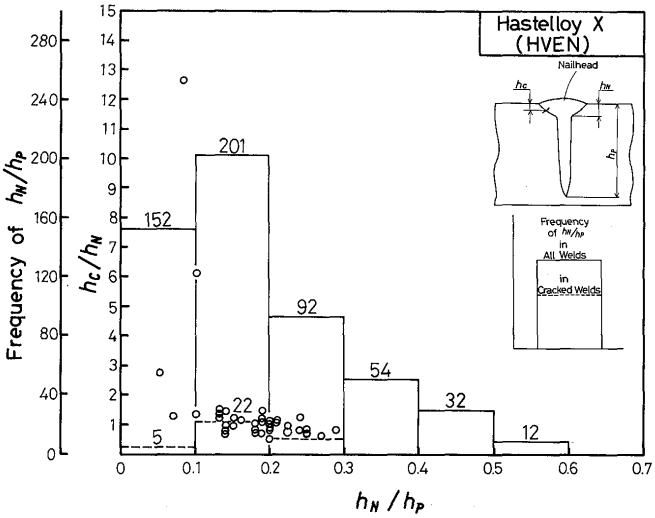

Fig. 11 Effect of h_N/h_P and h_c/h_N on Microcrack

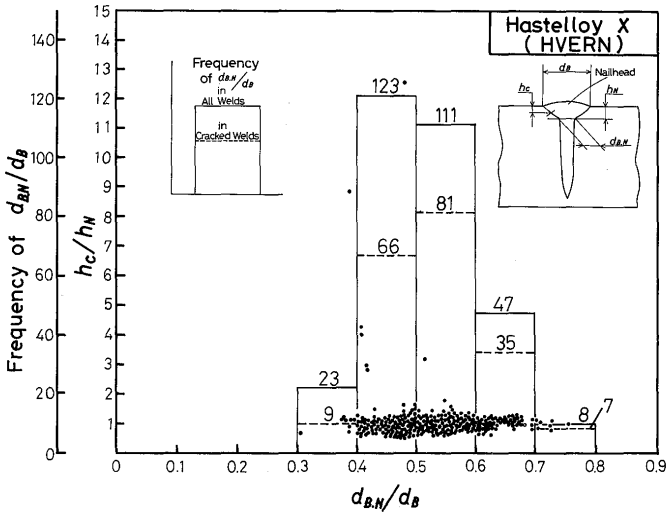

Fig. 13 Effect of $d_{B.N}/d_B$ and h_c/h_N on Microcrack

scattered around h_c/h_N of 1.0 as in Fig. 10 and called nailhead crack. In this figure, the frequency of h_N/h_P in all the welds and that in the cracked welds are also noted with the solid line and dotted line respectively. However, there is no clear correlation between this frequency and h_N/h_P.

In HAEN, HAEM and HVEN, not so sensitive to the microcrack as the above-mentioned three superalloys, similar tendency was also seen as shown in Fig. 11.

In Incoloy 800, microcracks are irregularly distributed regardless of h_c/h_N as shown in Fig. 12.

Fig. 13 shows the typical example in which microcrack is arranged on $d_{B.N}/d_B - h_c/h_N$ diagram (where, $d_{B.N}$: min. width of nailhead part, d_B: bead width at the top surface). In this figure, the frequency of $d_{B.N}/d_B$ in all the welds and that in the cracked welds are also noted with the solid line and dotted line respectively.

From this figure, it may be recognized that the microcrack comes to occur easily with the increase of $d_{B.N}/d_B$. Similar tendency was also shown in case of Inconel 617, Incoloy 800 and Incoloy 807.

5. Conclusion

The effect of the welding conditions on some characteristics of electron beam weld bead of the heat-resistant superalloys for the nuclear plants was herein investigated systematically. The obtained conclusion may be summarized as follows.

1) The weld defects were R-porosity at the root of the penetration and microcrack observed continuously in the interdendritic boundary of weld metal and the grain boundary of heat affected zone, which was nearly perpendicular to the fusion boundary.

2) R-porosity occurred within the individual areas on w_B-a_b diagram. Superalloys could be evaluated in the susceptibility to the R-porosity in terms of $\dot{S}_p$ and Δa_b. Fe-base superalloy was generally more susceptible to the R-porosity than Ni-base superalloy.
3) Superalloys could be evaluated in the sensitivity to the microcrack in terms of the critical line on w_b-v_b' diagram. Microcracks did never occur by limiting the welding conditions.
4) It was recognized from the effect of the heat input on the microcracking percentage that microcrack was apt to occur at the heat input larger than the critical value which was herein defined by q_{cr}. In terms of this critical heat input to avoid microcrack q_{cr}, superalloys are below placed in the order of less susceptibility to the microcrack.
(SUS316, Inconel 625), HAEM, HAEN, (HVEN, Inoloy 800), Incoloy 807, (HVERN, Inconel 617)
In Inconel 625 and SUS316, no microcrack did occur.
5) There was no clear correlation between the microcrack and penetroparameter P_p. Most microcracks were apt to occur when h_c/h_N came near to 1.0. These microcracks came to occur easily with the increase of $d_{B.N}/d_B$.

References

1) Y. Arata, K. Terai, S. Matsuda et al, "Study on Characteristics of Weld Defect and its Prevention in Electron Beam Welding (Report I) – Characteristics of Weld Porosities –", IIW Doc. IV-112-73 (1973)
2) Y. Arata, K. Terai, S. Matsuda et al, "Study on Characteristics of Weld Defect and Its Prevention in Electron Beam Welding (Report II) –Some Metallurgical Features of Weld Porosities –" IIW Doc. IV-147-74 (1974)
3) Y. Arata, K. Terai, S. Matsuda et al, "Study on Characteristics of Weld Defect and Its Prevention in Electron Beam Welding (Report III) – Characteristics of Cold Shuts –" Trans. of JWRI, Vol. 3 (1974) No. 2, p.81~88
4) J. D. Russel, A. J. Rodgers and R. J. Stearn, "Electron-beam welding of structural steels", Metal Construction & British Welding Journal, Vol. 6 (1974), No. 10, p.307~312
5) M. J. Bibby, J. A. Goldak and G. Burbidge, "Cracking in Restrained EB Welds in Carbon and Low Alloy Steels", Welding Journal, Vol. 54 (1975), No. 8, p.2535~2585
6) Y. Arata, "Terms and Definitions proposed from Japan" IIW, 1972
7) Y. Arata, M. Tomie, K. Terai et al, "Shape Dicision of High Energy Density Beam" Trans. of JWRI, Vol. 2 (1973), Nol 2, p.131~146